Modeling, Identification and Control, Vol. 44, No. 1, 2023, pp. 1–16, ISSN 1890–1328

Effect of Electrification on the Quantitative Reliability of an Offshore Crane Winch in Terms of Drive-Induced Torque Ripples

Mohamed Yousri Georg Jacobs Stephan Neumann

RWTH Aachen University, Institute for Machine Elements and System Engineering, Schinkelstr. 10, DE-52062 Aachen, Germany. E-mail: {yousri.mohamed,georg.jacobs,stephan.neumann}@imse.rwth-aachen.de

Abstract

Offshore crane winches are equipment installed on sea vessels and designed for accurate lifting and lowering of payloads at subsea levels in all conditions and are equipped with Active Heave Compensation (AHC) capabilities which keep the handled payload stable relative to the seabed. Due to logistical challenges and short maintenance windows imposed by sea conditions, maintenance of offshore crane winches in open sea is costly and time consuming, and its reliability is therefore of the highest importance. In recent times, electric drives for the actuation of the winch drum have seen a surge in popularity in favour of hydraulic drives owing to advances in control technologies of AC motors, as well as higher efficiency, lower noise and lack of an oil reservoir. In light of these changes and the importance of reliability, a study on the effect of the electrification (ie. switching from hydraulic to electric actuation) of offshore crane winches from a reliability viewpoint is necessary. In previous studies, it has been established that the different inherent properties of electric and hydraulic drives lead to torque ripples of different magnitudes and frequencies which may induce additional mechanical stresses in the drivetrain. The effects of these ripples on a system level have so far only been studied from a Noise-Vibration-Harshness (NVH) viewpoint in applications where driver comfort takes precedence in design (ex. electric vehicles, tractors). In this paper, these drive-induced ripples are simulated for common electric and hydraulic drive configurations used in offshore crane winches, and their effect on the reliability of the driven gearbox, as the most critical component in the drivetrain, is analysed. It was found that electric drives produce in general ripples of smaller magnitude (between 0.44% and 1.07% of static torque for electric compared to between 3.12% and 3.30% for hydraulic), which enhances the reliability of the driven gearbox (1.25% to 3.44% reduction in lifetime due to electric ripples, and 9.29% to 9.67% due to hydraulic ripples in comparison to an ideal torque source with no ripples). However, depending on the design and number of pumps in use, the size of the hydraulic torque ripple can have a wider range of between 1.31% and 7.69% and the subsequent reduction in lifetime compared to the ideal case ranging between 4.07% and 21.37%.

Keywords: Reliability, Offshore, Winch, Electrification, Electric, Hydraulic, Drive

1 Introduction

Offshore crane winches are equipment installed on sea vessels and designed for accurate lifting and lowering of payloads at subsea levels in all conditions, including temperatures down to -40°C with working depths of up to 4,000 m and a safe working load capacity of up to 600 tonnes (MacGregor, 2019) and are in most cases equipped with Active Heave Compensation (AHC) capabilities which compensate the heave motion of the

doi:10.4173/mic.2023.1.1

ship by rotating the winch drum with the same magnitude but opposite direction of heave motion (resulted from sea waves) in order to decouple the carried payload from the ship motion and keep the payload motionless relative to seabed. To actuate the winch drum, hydraulic or electric drives are commonly used. A simplified schematic of an AHC offshore crane winch can be seen in Figure 1.

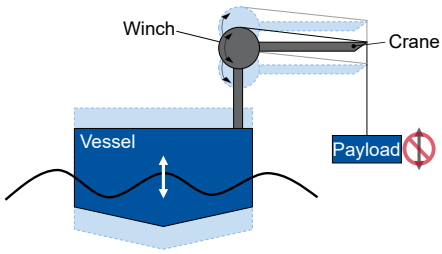

Figure 1: Simplified schematic of an AHC offshore crane winch

Due to the large financial risk associated with its failure in open sea and the logistical difficulty and cost of its maintenance, reliability of the offshore crane winch comes at the forefront of the design and maintenance processes of its drivetrain. Therefore, knowledge of different system influences on the drivetrain reliability is necessary, among which is the type of drive used to actuate the winch. Although electric-driven winches have been around for a while, they have recently seen a surge in popularity owing to advances in control technology which made using AC motors possible with high efficiency (70 to 85% peaks) and other advantages compared to hydraulic drives such as lack of oil reservoir and lower noise (Farsakoglu et al., 2022). Due to the recent commonality of use of both types of drives in offshore crane winches, a comparison of their effects on the system from a reliability viewpoint has not been studied before, where the electric-driven variant is particularly not studied enough (Woodacre et al., 2015). A previous comparison of the effects on reliability of an offshore crane winch as a result of another new trend (ie. opting for fibre instead of steel ropes for handling of the palyoad) was studied in (Yousri et al., 2020).

System simulations of the offshore crane winch have been made in (Bjonnes and Moe, 2012), where it was found that an all-electric offshore crane winch was better at controlling the winch drum motion while minimizing backlash than a similar hydraulic crane winch. Subsequent effect of this on the reliability of the system was not studied. In (Gu et al., 2012) a simulation model of a hydraulic active heave compensation system was developed and in (Aly, 2012), it was found that it is difficult to achieve high-precision tracking performance in hydraulic offshore crane winches using only linear PID controllers due to the high nonlinearities in the system, and a Model Reference PID (MR-PID) control strategy was proposed, which is an adaptive control methodology that computes control actions to make a non-linear controlled system track the behavior of a given reference plant model (Model Reference) to improve the performance of a PID controller. Other papers were focused on developing advanced control techniques like Model Predictive Control for AHC winches, which relies on a system model to determine optimal controller output by solving a quadratic optimization problem in order to reduce the control phase lag inherent in PID-controlled systems (Entao et al., 2009) (Deppen et al., 2011).

Pertaining to the breadth and depth of research done into winch compensation, and the availability of advanced control techniques which can achieve almost perfect compensation performance, the issue of compensation will not be the topic of this paper and equally adequate control performance will be assumed for both hydraulic and electric drives. Once this is established, hydraulic and electric drives are known to produce dynamic torque ripples that are a function of the inherent characteristics of their components (ex. axial piston pumps, frequency converters). These ripples may induce additional stress on the drivetrain components, thereby reducing their lifetime (Xia et al., 2011) and have been the subject of numerous studies (Guan et al., 2014) (Zhang et al., 2017) (Kennel et al., 2004) (del Toro et al., 2005) that attempt to numerically simulate them as well as reduce their size for both hydraulic and electric drives. The effects of these ripples on a system level have been studied from a Noise-Vibration-Harshness (NVH) viewpoint in applications where low noise and driver comfort are most important such as in agricultural tractors (Pasch et al., 2020) and electric vehicles (Mao et al., 2017). It was found in (Pasch et al., 2020) that pressure pulsations from the hydrostatic unit propagate through the tractor's structure, causing vibration and noise. In (Mao et al., 2017), it was found that the torque ripple of an electric vehicle's in-wheel PMSM motor is prone to arouse horizontal vibration contributing to NVH problems in the vehicle.

The objective of this paper is to quantify the torque ripple behaviour of typical electric and hydraulic drive configurations used in offshore crane winches in terms of magnitude and give an evaluation of the ripple influence on the reliability of the driven gearboxes, as

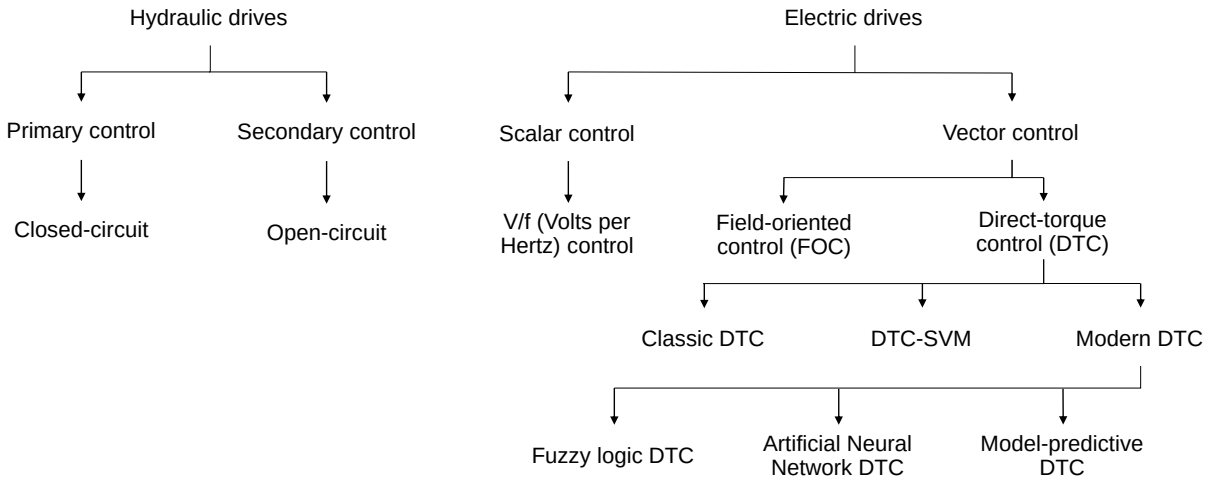

Figure 2: Classification of commonly used drives in offshore crane winches

the most critical components of the drivetrain (Woell et al., 2017). Subsequentially, a conclusion can be made about the extent of improvement in reliability resulting from electrification of the winch in terms of the ripples. In the next subsections, common electric and hydraulic drive configurations used in offshore crane winches are discussed and the underlying theory behind the torque ripples explained. An overview of drives used in offshore crane winches can be seen in Figure 2.

1.1 Hydraulic drives

Ever since the first commercial AHC offshore crane was rolled out in the early 1980s (Sullivan et al., 1984), hydraulic drives were used for actuation and are up to this point the more commonly used type of drives as they provide the highest power to weight ratio of any actuator currently on the market which can be appealing when deck space is limited. Since they are well-established, their troubleshooting and repair is also easier in comparison to electric drives. However, problems such as lower efficiency and oil leakage make it more attractive to switch to electric drives in light of environmental regulations, hence the recent popularity of the latter. As seen in Figure 2, traditional hydraulic drives in offshore crane winches come in the following forms:

- Primary controlled closed-circuit (Hydraulic 1), where the pumps have variable displacement and are controlled to supply as much flow as needed to rotate the winch drum at a given time. The advantage of this variant over the latter is a higher efficiency due to the oil staying within the closed system and not being lost to the tank when the flow is not needed at a given moment. The setup of this variant allows for energy regeneration as the motors/pumps can operate in the four quadrants. A simplified schematic of this variant can be seen in Figure 3.

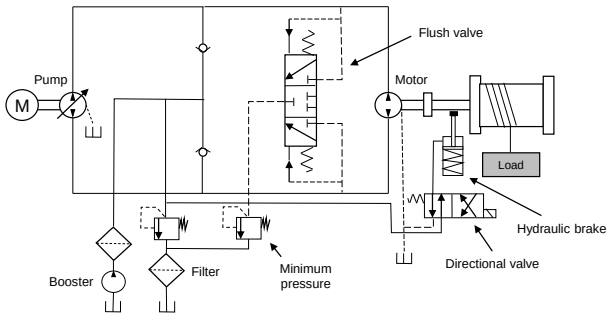

Figure 3: Schematic of a primary controlled closed-circuit hydraulic drive

- Secondary controlled open-circuit form (Hydraulic 2), where fixed-displacement pumps supply oil at a constant pressure to variable-displacement motors which are controlled by a directional valve to actuate the winch drum with the desired speed and direction. The advantage of this variant over the former is faster response times since the motors themselves are controlled (which are closer to the load) (Albers, 2010). A simplified schematic of this variant can be seen in Figure 4.

The most important components which make up a hydraulic drive in offshore crane winches are the axial piston pumps and motors, whose design and working principle lead to large flow ripples as each piston

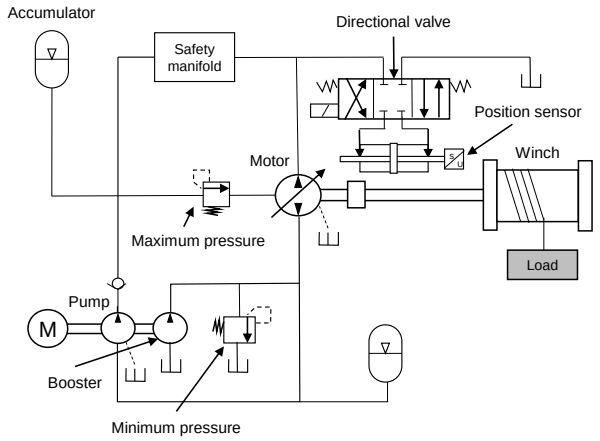

Figure 4: Schematic of a secondary controlled open-circuit hydraulic drive

in the axial piston machine periodically connects and disconnects to the suction and discharge areas of the valve plate (see Figure 5). These flow ripples can be divided into three components, namely the kinematic flow, inverse flow from discharge into piston chamber and leakage flow. These components as well as their governing equations are explained below.

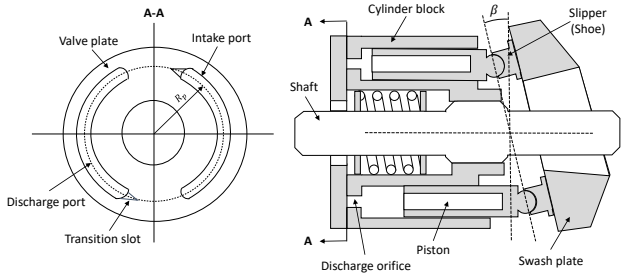

Figure 5: Schematic of an axial piston pump

Kinematic flow

The kinematic portion of the flow ripple for each individual piston in the axial piston machine results from the rotation of the piston around the drive shaft axis as the fluid rushes into the piston during the suction half while it is connected to the suction port, and then rushes out of the piston during the discharge half as it connects to the discharge port, completing one cycle, without considering the effect of the discontinuity in the valve plate geometry represented in the gaps between the suction and discharge ports. Eq. (1). governs this kinematic flow.

$$Q_{ki} = \frac{\omega \pi d^2 R_p}{4} tan\beta \sum_{k=0}^{n-1} sin(\omega t - k\alpha) \qquad (1)$$

Here, Q_{ki} is the kinematic flow for individual piston i in the axial piston machine. As seen in the equation, the kinematic flow is proportional to the inclination angle β of the swash plate, the piston pitch radius R_p, the drive shaft rotational speed ω and the piston diameter d. The kinematic flow component makes up around 8% of the total magnitude of the flow ripple according to (Zhang et al., 2017).

Inverse flow

As a piston initially connects with the discharge port, there is a significant pressure difference between the pressure P_{pi} inside the piston chamber, which is still at the low suction pressure, and the pressure in the discharge chamber P_d. This pressure difference leads to an inverse flow from the discharge chamber into the piston, and is considered the most signifcant element contributing to the flow ripple, making up around 88% of its total size (Zhang et al., 2017) and is the focus point of most research attempting to simulate the flow ripples accurately including fluid compressibility and design features aimed at reducing it such as a damping hole (Guan et al., 2014) which pre-pressurizes the fluid before connecting to the discharge chamber or a silencing groove (Mandal et al., 2008) which smoothens the pressure gradient.

$$Q_{pi} = \sqrt{\frac{2\,|P_d - P_{pi}|}{\rho}} C_d A_{kd} sign(P_d - P_{pi}) \qquad (2)$$

Eq. (2). governs this inverse flow from the discharge port into the piston for the entire cycle of rotation of a single piston, and is a classic orifice equation taking into consideration the variation of the discharge area A_{kd} relative to the valve plate geometry.

Leakage flow

Inside an axial piston pump, some leakage flow occurs which helps lubricate parts which have relative motion and it makes up around 4% of the total flow ripple size (Zhang et al., 2017). As modelled by (Ivantysyn and Ivantysynova, 2003), there are three types of leakage which happen. First is the leakage flow through the clearance between the piston and the cylinder block which can be expressed as

$$Q_{lci} = \frac{\pi r h_g^3}{6\mu l_{cp}} (P_{pi} - P_c) \qquad (3)$$

where h_g is the oil film thickness between the piston and the cylinder block, μ is the kinetic viscosity of the fluid, l_{cp} is the instantaneous overlap length of the piston and the cylinder block and P_c is the pressure of the case chamber. The second type of leakage flow is the leakage between the slipper and the swash plate and is calculated as

$$Q_{lsi} = \frac{\pi d_{lh}^4 \delta_s^3}{\mu[6d_{lh}^4 ln(R_s/l_s) + 128\delta_s^3 l_p]}(P_{pi} - P_c) \quad (4)$$

where d_{lh} is the diameter of the piston leakage hole, d_s is the clearance between the slipper and the swash plate, R_s and r_s are the outer and the inner radii of the slipper and l_p is the total length of the piston. The third and final type of leakage happens through the clearance between the cylinder block and the valve plate and is calculated as

$$Q_{lv} = \frac{\delta_v^3}{12\mu}\left[\frac{1}{ln(R_2/R_1)} + \frac{1}{ln(R_4/R_3)}\right](P_d - P_c) \quad (5)$$

where δ_v is the clearance between the valve plate and the cylinder block, R_1 and R_2 are the inside and outside radii of the inside valve plate seal ring, and R_3 and R_4 are the inside and outside radii of the outside valve plate seal ring. Finally, the total leakage per individual piston can be calculated as $Q_{li} = Q_{lci} + Q_{lsi}$, where Q_{lv} can only be considered when calculating leakage for the whole pump.

Piston chamber instantaneous pressure

During the course of one full rotation of a piston around the drive shaft axis, the control fluid volume inside the piston varies as a result of the variation of the three flow components mentioned previously which leads to a time-dependent variation in piston chamber pressure. Eq. (6). is the differential equation for the pressure-rise-rate in the piston chamber where E is the fluid bulk modulus and V_{pc} is the instantaneous piston chamber volume.

$$\frac{dP_{pi}}{dt} = \frac{E}{V_{pc}}(Q_{ki} + Q_{pi} - Q_{li}) \quad (6)$$

$$V_{pc} = V_0 - A_p R_p tan\beta(1 - cos\varphi) \quad (7)$$

Here, V_0 is the initial piston volume, A_p is the piston area and φ is the angle of rotation of the cylinder block.

Total flow, pressure and torque

Solving the set of differential and algebraic equations eq. (1). to eq. (7). yields the individual piston flow and pressure. To calculate the total discharge flow of the pump (ie. flow going from piston into the discharge chamber), the absolute value of the individual inverse flows of all pistons are to be summed, where n is the number of pistons in the pump.

$$Q_p = \sum_{i=1}^{n} |Q_{pi}| \quad (8)$$

Depending on the load carried and flow required, and other system parameters such as pipe dimensions, a pressure arises in the pipes transmitting flow to the motors as a result of the system's resistance to the flow. Proportional to this pressure is the output torque of the motors, as seen in eq. (9). below. It can be thus seen how the pump flow ripples will be translated into output torque ripples at the motors.

$$T_h = \frac{PD_m\eta_m}{20\pi} \quad (9)$$

Here, P is the pressure, D_m is the motor displacement and η_m is the motor efficiency.

1.2 Electric drives

There is evidence that electric-driven winches (non-AHC) have been around as early as 1970, which were using DC motors a while before the advancements in motor control technology made it possible to control AC motors dynamically on a mass scale. The first offshore crane winch driven by an AC motor dates back to the early 1990s (Woodacre et al., 2015), and were likely driven by a Variable Frequency Drive (VFD) called the scalar VFD, which maintains a fixed voltage to frequency ratio to control speed and correct for reduced motor impedance at lower frequencies. Scalar VFDs cannot control current (and hence torque) independently, and thus are not suitable for control of AC motors in low speed/high torque applications requiring high dynamics (Busca, 2010), such as in offshore crane winches. Modern electric-driven offshore crane winches use vector VFD techniques such as Field Oriented Control (FOC) and Direct Torque Control (DTC) which can independently control torque and flux thus resulting in more accurate control in dynamic applications. Modern VFDs also allow for energy regeneration which leads to higher efficiency. Among the two methods, Direct Torque Control is the control method of choice for various offshore crane winch drives available on the

market (ABB, 2013) (Danfoss, 2010) due to its higher robustness in controlling quick torque dynamics and simpler parameterization, where the drive is not sensitive to parameter changes as well as being a sensorless method that does not need an external encoder to measure speed and position which saves space and cost (Begh and Herzog, 2018). In the following subsections, the working mechanism of Direct Torque Control will be explained, as well as how it results in torque ripples. Trials to reduce these ripples in previous research will also be mentioned.

DTC and torque ripples

DTC is a method of controlling AC drives that was proposed by (Takahashi and Noguchi, 1986) and (Depenbrock, 1988), as a result of a quest to avoid coordinate transformation and design a control strategy that is independent of the machine parameters as is the case with FOC. What is being controlled here is an Induction Motor, whose governing equations can be referred to in (Slemon, 1989). The aim of DTC is to control and regulate the electromagnetic torque and flux of the machine in a decoupled manner. In order to do that, the torque and flux of the motor are first estimated from the voltage and current as follows in eq. (10). to eq. (13). below.

$$\hat{\psi}_s = \sqrt{\hat{\psi}_{s\alpha}^2 + \hat{\psi}_{s\beta}^2} \tag{10}$$

$$i_s = \frac{1}{\sigma L_s}(\psi_s - \frac{L_m}{L_r}\psi_r), \;\; \sigma = 1 - \frac{L_m^2}{L_s L_r} \tag{11}$$

$$T_{em} = \frac{3}{2}p(\hat{\psi}_s \times i_s) = \frac{3pL_m}{2\sigma L_s L_r}\,|\psi_s|\,|\psi_r|\,\theta \tag{12}$$

where the stator flux components in the reference frame (α, β) are

$$\begin{aligned} \hat{\psi}_{s\alpha} &= \int_0^t (v_{s\alpha} - R_s i_{s\alpha})dt \\ \hat{\psi}_{s\beta} &= \int_0^t (v_{s\beta} - R_s i_{s\beta})dt \end{aligned} \tag{13}$$

and the sector where the stator flux lies is

$$\theta_s = \arctan(\frac{\hat{\psi}_{s\alpha}}{\hat{\psi}_{s\beta}}) \tag{14}$$

Afterwards, the error between the estimated torque and flux T_{em} and ψ_s and the reference values T_{em^*} and ψ_{s^*} provided by the speed control loop is measured with the goal of holding the magnitude of the torque and flux within a narrow hysteresis band around the reference values. The hysteresis comparator of the flux (two-level) decides then if the flux needs to be increased (1) or decreased (-1) while that of the torque (three-level) decides if the torque should be increased (1), held at the same level (0) or decreased (-1). These signals are then the input to the switching table (see Table 1), together with signals of the stator flux sector θ_s to produce the appropriate inverter switching sequence S_a, S_b, S_c to bring the flux and torque towards their reference values. The switching sequence produces the voltage vector in the (α, β) plane necessary to achieve that (see Figure 6). This process can be imagined more clearly by looking at Figure 7.

Table 1: Switching table of a classic DTC drive (El Ouanjli et al., 2019a)

Sector		1	2	3	4	5	6
H_s	H_{Tem}	Voltage vector					
1	1	v_2	v_3	v_4	v_5	v_6	v_1
	0	v_7	v_0	v_7	v_0	v_7	v_0
	-1	v_6	v_1	v_2	v_3	v_4	v_5
0	1	v_3	v_4	v_5	v_6	v_1	v_2
	0	v_0	v_7	v_0	v_7	v_0	v_7
	-1	v_5	v_6	v_1	v_2	v_3	v_4

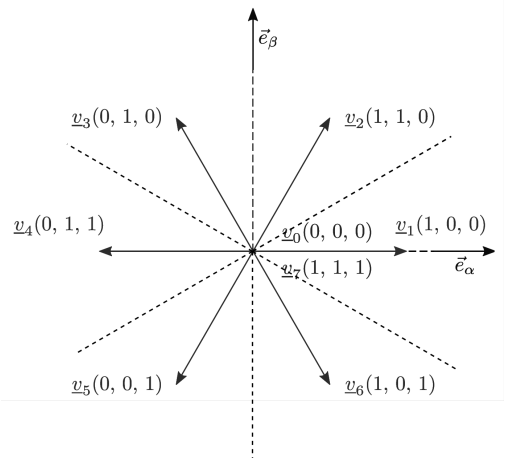

Figure 6: Voltage vector in the (α, β) plane (Begh and Herzog, 2018)

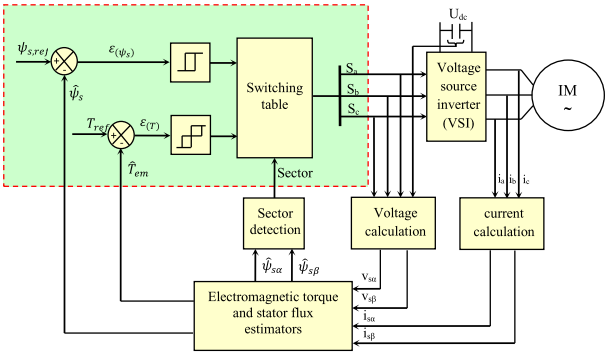

Figure 7: Simplified schematic of a classic DTC drive (El Ouanjli et al., 2019a)

Trials at reducing torque ripples

The method that was explained in the previous subsection is the so-called Conventional Direct Torque Control (C-DTC) method, which despite of its simplicity is characterized by high torque ripples due to its highly variable switching frequency where lower switching frequencies particularly cause this problem. In order to reduce the torque ripples, several methods were developed in recent years. In this subsection, two of these methods will be shortly discussed, one older method Direct Torque Control with Space Vector Modulation (DTC-SVM) and one more modern, based on Artificial Intelligence, Fuzzy Logic Direct Torque Control (FL-DTC). DTC-SVM is an adaptation to the C-DTC method where the torque and flux hysteresis comparators are replaced by PI controllers and the switching table is replaced by a Space-Vector-Modulator (SVM) to supply the correct switching states to the Voltage Source Inverter, which ensures a constant switching frequency, thus avoiding the problem with large torque ripples associated with lower swtiching frequencies common to C-DTC. A more detailed explanation of this method can be referred to in (Hiba et al., 2013). In (De Klerk and Saha, 2022), it was found that DTC-SVM leads to an average reduction of 26 % in the size of the torque ripple in an electric vehicle compared to C-DTC. Likewise, FL-DTC is a more modern adaptation to C-DTC where the switching table and hysteresis comparators of C-DTC are replaced with new selection tables based on a Fuzzy Logic Controller (FLC) to improve dynamic performance by producing vector voltage that drives the flux and torque to their set values optimally with smaller fluctuations. A more detailed explanation of this method can be referred to in (El Ouanjli et al., 2019b). Reasons why Fuzzy Logic can lead to smaller torque ripples include the ability to limit and adjust the torque hysteresis band in real time according to the slope of variation of the estimated torque (Uddin and Hafeez, 2010) as well as generally faster response in bringing the torque and flux to their set values. It was found in (El Ouanjli et al., 2019b) that using Fuzzy Logic leads to a reduction of 47.7% in torque ripples compared to C-DTC. As can be seen, although modern torque ripple reduction techniques have been proved to reduce electromagnetic torque ripples significantly, they still cannot eliminate them completely as of yet.

2 Methods

In order to simulate the hydraulic and electromagnetic torque ripples and their effect on the reliability of the offshore crane winch, a system model of the winch is built from the components described in the following subsections. In subsection 2.6, the simulated load case will be also described.

2.1 Winch

In Table 2, the properties of the simulated example offshore crane winch are laid out. The parameters of the drives shown in Table 3 to 6 are then calculated such that they are able to actuate the winch at the maximum load and compensation speed shown below, however these calculations are out of the scope of this paper.

Table 2: Offshore crane winch properties

Parameter	Unit	Value
Carrying capacity	$tons$	150
Max. working depth	m	3000
Max. AHC speed	m/s	2
Winch radius	m	1.15
Winch mom. of inertia	$kg \cdot m^2$	151720

2.2 Hydraulic drives

In this paper, the primary controlled closed-loop (Hydraulic 1) configuration and the secondary controlled open-loop (Hydraulic 2) configurations were chosen to represent the hydraulic drive. The pumps/motors are modelled based on physical components in the Simscape environment of MATLAB/Simulink which are built using the well-established and validated equations for pump flow laid out in subsection 1.1. The parameters of the simulated hydraulic drive are laid out in Table 3 to 5. In Figure 8, the build-up of the flow modelling for one piston, connected to a swash plate whose inclination is controlled to vary the pump (primary) or motor (secondary) displacement according to

flow need is shown. The piston is also connected to the two-halves of the valve plate, one for suction and the other for discharge.

Table 3: General hydraulic drive parameters

Parameter	Symbol	Unit	Value
No. of pumps	-	-	9
No. of motors	-	-	20
Oil viscosity	μ	cSt	34.47
Oil bulk modulus	E	GPa	1.47
Pipe length	l_p	m	10
Pipe diameter	d_p	m	0.155

Table 4: Axial piston pump parameters

Parameter	Symbol	Unit	Value
Pump displacement	D_p	cm^3/rev	1000
No. of pistons	n	-	5
Piston area	A_p	m^2	0.001
Piston stroke	S_p	m	0.2
Piston pitch radius	R_p	m	0.2
Discharge orifice radius	r_o	m	0.005
Phase angle	α	rad	1.257
Discharge coefficient	C_d	-	0.65
Transition slot area	A_{ts}	m^2	1e-6

Table 5: Axial piston motor parameters

Parameter	Symbol	Unit	Value
Motor displacement	D_m	cm^3/rev	250
No. of pistons	n	-	5
Piston area	A_p	m^2	0.001
Piston stroke	S_p	m	0.05
Piston pitch radius	R_p	m	0.05
Discharge orifice radius	r_o	m	0.005
Phase angle	α	rad	1.257
Discharge coefficient	C_d	-	0.65
Transition slot area	A_{ts}	m^2	1e-6

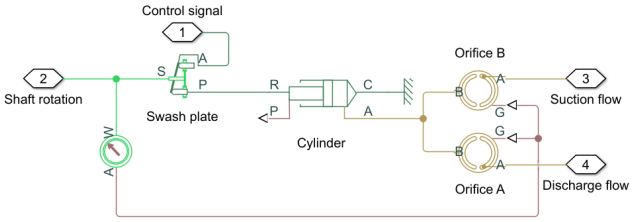

Figure 8: Flow modelling of a single piston using Simscape components

configuration. The building block of the drive is the pre-built MATLAB/Simulink block AC4 as described in (Mathworks, 2012), which comes in both C-DTC and DTC-SVM variants, but can also be made to work as FL-DTC when replacing the hysteresis comparators and switching tables of the C-DTC variants with Fuzzy Logic Controllers. The Fuzzy Logic Controller used in the simulation was built according to the method and parameters in (El Ouanjli et al., 2019b).

Table 6: General electric drive parameters

Parameter	Symbol	Unit	Value
Nominal power	P_n	kW	120
No. of pole pairs	p	-	2
Stator resistance	R_s	ohms	0.01485
Rotor resistance	R_r	ohms	0.01485
Stator inductance	L_s	H	0.0003
Rotor inductance	L_r	H	0.0003
Mutual inductance	L_m	H	0.01046
Speed control - P gain	P_v	-	30
Speed control - I gain	I_v	-	200

Table 7: C-DTC specific parameters

Parameter	Unit	Value
Max. switching frequency	Hz	20000
Torque control - hys. bandwidth	Nm	0.5
Flux control - hys. bandwidth	Wb	0.01

2.3 Electric drives

For the electric drive, the three variants of Direct Torque Control (DTC) drives described in subsection 1.2 are simulated with the general parameters in Table 6. Variant-specific parameters are shown in Table 7 for C-DTC and in Table 8 for DTC-SVM. As with the hydraulic drive, the electric variants have 20 motors each, connected together in a master-follower

2.4 Gearbox

In this paper, the gearbox is modelled as a simple rigid beam, where the component loads are calculated from the drive torque using transfer functions derived from solving equilibrium of moments and forces on each of the shafts. The gearbox modelled is a two-stage planetary gearbox with an additional spur gear stage which connects to the ring gear on the outside of the winch

Table 8: DTC-SVM specific parameters

Parameter	Unit	Value
Switching frequency	Hz	20000
Torque control - P gain	-	1.5
Torque control - I gain	-	100
Flux control - P gain	-	250
Flux control - I gain	-	4000

drum as seen in Figure 9. The winch drum, rope and payload are modelled as masses and rotational inertias.

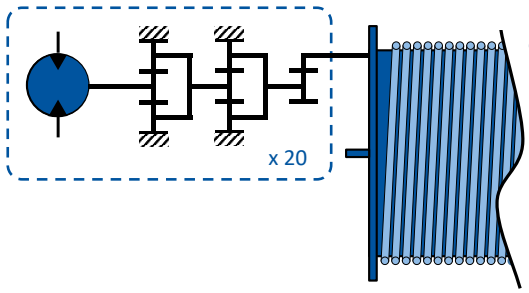

Figure 9: Schematic of the crane winch drivetrain

2.5 Lifetime model

When the component loads are calculated from the gearbox model, they are then used to calculate the component, as well as the system (ie. gearbox) lifetime. The lifetime calculation of mechanical components is based on the analysis and comparison of the stress and strength of the component. The strength or load capacity of components is evaluated using available standards (Bearings: DIN ISO 281, Gears: DIN 3390). The results of the load capacity calculation are usual S-N curves. The lifetime model used in this paper is based on (Neumann et al., 2016), where the component loads are transformed into load spectrums using a counting method specific for oscillating bearings (Woell et al., 2018). By applying a damage accumulation hypothesis on stress (load spectrums) and strength (S-N curves) the damage sum for each investigated component and subsequently the expected lifetime for each component can be determined (Woell et al., 2017). A schematic of the lifetime calculation methodology used can be seen in Figure 10. From the calculated lifetime, the failure probability of each component over time can be described using a Weibull distribution with eq. (15).

$$F(t) = 1 - e^{-\left(\frac{t-t_0}{T-t_0}\right)^b} \tag{15}$$

Here, T is the characteristic lifetime of the component, t_0 is the failure-free time and b is the component-specific exponent. Later, the system (ie. gearbox) lifetime can be calculated from the individual component lifetimes with eq. (16).

$$F_{sys}(t) = 1 - \prod_{i=1}^{n}(1 - F_i(t)) \tag{16}$$

2.6 Load cases

For an equal comparison between the simulated drives, the winch is subject to the following load cases shown in Tables 9 and 10 for all simulations. The winch is subject to sea waves that are assumed to be sinusoidal in shape in order to make the analysis of the ripples easier. In the first load case, the sinusoidal wave represents a smooth sea wave produced by a wind speed of Level 2 on the Beaufort scale (light breeze) and in the second load case, the sinusoide represents a moderately high wave produced by a wind speed of Level 5 on the Beaufort scale (strong breeze) which puts the AHC system near its speed limit.

Table 9: Carried load and working depth

Parameter	Symbol	Unit	Value
Payload mass	M	kg	50000
Rope specific mass	m_{spec}	kg/m	25.49
Working depth	L	m	3000

Table 10: Load cases

Parameter	Load case 1	Load case 2
Wind speed	2-3 m/s	9-11 m/s
Wave amplitude	0.3 m	2.4 m
Wave period	10 s	6 s

3 Results and Discussion

In this section, the ripple size and effect on the driven gearbox lifetime (in comparison to an ideal torque source with no ripples) will be shown and discussed in subsection 3.1 for the main use case defined in section 2. Afterwards, the results of the sensitivity analysis made on the parameters of the primary controlled hydraulic drive (Hydraulic 1) is shown in subsection 3.2.

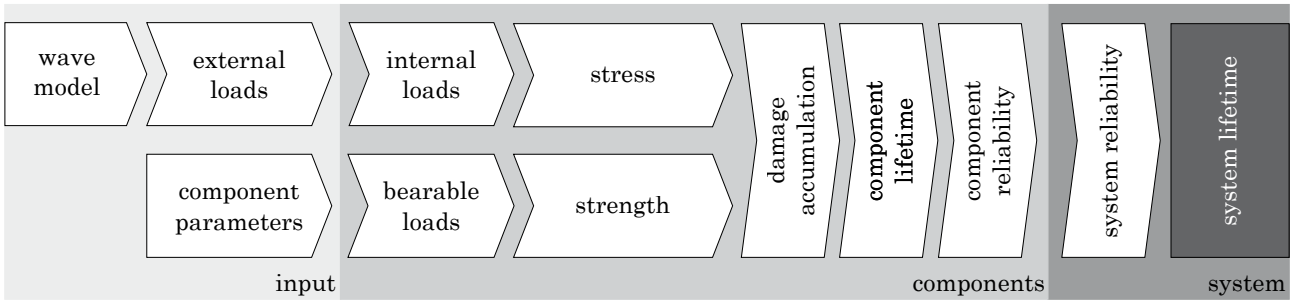

Figure 10: Reliability calculation approach (Neumann et al., 2016)

3.1 Main load cases

In Table 11, the ripple size, calculated as a percentage of the static output torque of the motor as well as the normalized lifetime of the driven gearbox (in comparison to when using an ideal torque source to actuate the winch) for all the simulated drive variants with the parameters defined in section 2 are shown. In Figure 11, a 40 second long snapshot of the motor output torques for the Hydraulic 1, FL-DTC and Ideal variants is shown for the sake of comparison. From Table 11 and Figure 11, it can be seen for Load case 1 that for the electric drive variants, the ripple size ranges between 0.44% for the FL-DTC variant to 1.07% for C-DTC with a subsequent reduction in lifetime of 1.25% to 3.44% compared to the ideal case. The difference in size of torque ripples among the electric drive variants falls in line with what is expected from the torque ripple reduction techniques discussed in 1.2. For the hydraulic drive variants on the other hand, a ripple size of 3.12% is seen for the Hydraulic 2 variant and 3.30% is seen for the Hydraulic 1 variant with a subsequent reduction in the driven gearbox lifetime of 9.29% and 9.67% respectively. The reason for the difference is that the additional torque spikes (see Figure 11) seen in the Hydraulic 1 variant when changing the winch's direction of rotation are not present with the Hydraulic 2 variant due to a faster response time of the latter. As for Load case 2, the same trends persist although with slightly larger torque ripples resulting from lower quality in controlling the winch speed under higher wave acceleration, however this is merely a limitation of the simulation models used and should not arise under real conditions where controllers are designed to work with high accuracy under the full range of winch speed.

3.2 Sensitivity analysis

After establishing in subsection 3.1 that electric drives produce smaller ripples than hydraulic drives, it is necessary for a full picture to carry out a sensitivity analysis on the main design parameters of the hydraulic drive in order to see if it can get any close to electric drives in the size of its ripples when optimizing its design. Therefore in this subsection, a few parameters which are expected to have an influence on the hydraulic torque ripple are swept within their design boundaries to study their effect.

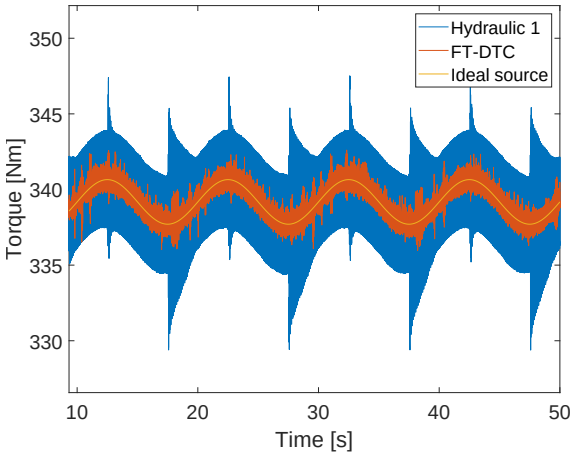

Figure 11: Motor output torque for Hydraulic 1, FT-DTC and Ideal variants (Load case 1)

Pipe diameter d_p

When thinking of parameters that can influence the size of the hydraulic torque ripples, the diameter of the piping transmitting the fluid in the drive is one of the most obvious, as it plays a role in determining the amount of resistance to fluid flow that there is in the system, and thus the pressure build-up. As a general recommendation, flow speed in the pressure pipes of a hydraulic drive should be kept in an optimal range between $u_{lower} = 7.25\ m/s$ and $u_{upper} = 9\ m/s$ when dealing with pressures up to 350 bar. From that, the range of pipe diameters that are considered a good compromise between low power losses and cost/size can be calculated from the following formula (Paul Forrer AG, 2011)

Table 11: Ripple percentage and influence on gearbox lifetime of the simulated drive variants

Drive	Load case 1		Load case 2	
	Ripple [%]	Lifetime [-]	Ripple [%]	Lifetime [-]
Ideal	0	1.0000	0	1.0000
FL-DTC	0.44	0.9875	0.73	0.9784
DTC-SVM	0.65	0.9808	0.94	0.9707
C-DTC	1.07	0.9656	1.91	0.9427
Hydraulic 2	3.12	0.9071	3.26	0.9056
Hydraulic 1	3.30	0.9033	3.42	0.9008

$$4.61\sqrt{\frac{q_{max}}{u_{lower}}} \leq d_p \leq 4.61\sqrt{\frac{q_{max}}{u_{upper}}} \qquad (17)$$

In order to achieve the maximum hoisting speed of the winch, a maximum flow of $q_{max} = 8813.35\ L/min$ through the piping is calculated. Substituting the speeds into the equation, we find that $0.145\ m \leq d_p \leq 0.165\ m$ is an optimal range for the pipe diameter. Therefore, the pipe diameter is sweeped within these boundaries in Table 12. From the results in Table 12, it can be seen that increasing the pipe diameter within the limits of what is considered optimal in terms of low losses and cost offers less resistance to flow in the system, and thus smaller pressure and subsequentially smaller torque ripples.

Table 12: Effect of hydraulic pipe diameter on ripples and gearbox lifetime

$d_p\ [m]$	Ripple [%]	Lifetime [-]
0.145	4.21	0.8753
0.150	3.81	0.8893
0.155	3.30	0.9033
0.160	2.84	0.9160
0.165	2.49	0.9259

The effect of sweeping the pipe diameter d_p can be more clearly visualized in Figure 13a. It can be seen that sweeping the pipe diameter within the limits calculated using eq. (17) leads to a deviation in lifetime of -3.10% and +2.50% from the original value.

Piston orifice radius r_o

One of the piston parameters that is expected to have a large influence on the ripples is the piston orifice radius r_o which connects the piston to the valve plate's dischage and suction chambers. The effect of this parameter on the ripple size and gearbox lifetime can be seen in Table 13.

Table 13: Effect of piston orifice radius on ripples and gearbox lifetime

$r_o\ [m]$	Ripple [%]	Lifetime [-]
0.003	1.31	0.9593
0.004	2.13	0.9351
0.005	3.30	0.9033
0.006	4.71	0.8639
0.007	5.03	0.8524
0.008	7.69	0.7863

As can be seen in the table, having a smaller orifice radius significantly reduces the ripple size (and thus influence on lifetime) theoretically as it leads to a smaller discharge area A_{kd}, which, as seen in eq. (2)., plays a role in the amount of inverse flow going into the piston chamber, where a smaller discharge area leads to a smaller inverse flow and thus a smaller flow ripple and subsequentially pressure and torque ripples. However, it is important to note that factors like difficulty and cost of manufacturing such small orifices as well as other phyiscal and design limitations are not considered here. Very small orifices can lead to cavitation or hinderence of flow as well as being difficult and costly to manufacture due to machining limitations. In Figure 13b, the effect of sweeping the orifice radius r_o can be more clearly visualized. It can be seen that the orifice radius has a more pronounced effect on lifetime than pipe diameter, where sweeping it within acceptable limits leads to a change in lifetime of the driven gearbox between -12.95% and +7.6% compared to the original value.

Pump asynchronization

Another parameter that can potentially influence the size of the hydraulic flow (and hence torque) ripple is how much in or out of phase the individual pumps in a hydraulic drive are running relative to one another, with an expectation that running every pump with a

180° phase shift (inverse) to the next pump can help reduce the ripples. In this subsection, the influence of this on the total flow as well as torque ripple in the simulated hydraulic drive 'Hydraulic 1' containing 9 pumps is investigated.

Table 14: Effect of pump phase shift on ripples and gearbox lifetime

Phase shift [°]	Ripple [%]	Lifetime [-]
0	3.30	0.9008
180	3.18	0.9071

As can be seen in the Table 14, the 180° phase shift only minimally reduces the size of the torque ripple and thus results in a slightly better lifetime. This can be explained by looking at the shape of the total pump flow Q_p for a single pump in Figure 12a, characterized by the double peak related to the pump's total kinematic flow Q_k as well as the periodic spikes related to the inverse flow when the pistons connect with the suction or discharge ports. In Figure 12b, the flows of Pump 1 and Pump 2 in the drive (which are out of phase) are shown side-by-side. It can be clearly seen that when added together, they will not cancel out as opposed to when using pumps with single pistons that would produce a more sinusoidal flow shape.

Figure 12c and Figure 12d show the total flow of all 9 pumps with no phase shift, and with 180° phase shift respectively. The phase shift results in a slightly smaller flow ripple amplitude as well as double the amount of periodic spikes related to the inverse flow. Between Figure 12a and Figure 12c, it can be seen that with 9 pumps, the flow of every individual pump is summed. From here, it can be suggested that whenever possible, using a smaller number of pumps can help reduce the size of the flow, and thus torque ripples. For example, for the first load case, it was calculated that only 3 pumps are necessary to provide enough flow to actuate the winch and achieve full heave compensation. In Table 15 and in Figure 13c, it can be seen that the ripple size decreases linearly when using less pumps simultaneously as less flow ripples of individual pumps are summed. However, in an application with heavy handled loads like the offshore crane winch, operating in environments with relatively high waves (North Sea), it is likely that the full capacity of pumps will need to be used at once for AHC compensation most of the time.

Table 15: Effect of number of pumps in use on ripple size and lifetime

No. of pumps [-]	Ripple [%]	Lifetime [-]
3	0.86	0.9733
4	1.32	0.9593
5	1.78	0.9453
6	2.24	0.9300
7	2.70	0.9198
8	3.16	0.9071
9	3.30	0.9033

4 Conclusion

In this paper, the theory behind drive-induced torque ripples for electric and hydraulic drives was introduced, after which the ripples were simulated for commonly used electric and hydraulic drive configurations in offshore crane winches and their effect on the crane winch's driven gearbox lifetime was studied. Finally, a sensitivity analysis was made for the hydraulic drive to study the extent to which their torque ripples can reduced in comparison to electric drive ripples. It was found that for the given use case and simulated drives, hydraulic torque ripples range from 1.31% to 7.69% in size as a percentage of the applied static torque, depending on the chosen design parameters, causing a subsequent reduction in lifetime of 4.07% to 21.37% compared to the ideal case. On the other hand, electric torque ripples range from 0.44% to 1.07 % in size, causing a subsequent reduction in lifetime of 1.25% to 3.44% compared to the ideal case. In addition, it was found that pump asynchronization in hydraulic drives does not significantly reduce the torque ripples, however using a smaller number of pumps when load demand allows can help reduce the size of the torque ripples. From these results, a conclusion can be made for the specific application and use cases simulated that switching from hydraulic to electric actuation of an offshore crane winch would lead to enhancing the lifetime of its drivetrain for the same size of gearbox components or would alternatively allow for using a downsized gearbox to achieve the same level of reliability as a result of the smaller, less damaging torque ripples of electric drives, thus potentially saving costs.

5 Future Work

So far the magnitudes of the drive-induced torque ripples and their effect on the driven gearbox's lifetime has been studied, assuming a gearbox with rigid components. For a more general conclusion on the effect of these ripples, it would be also interesting to study

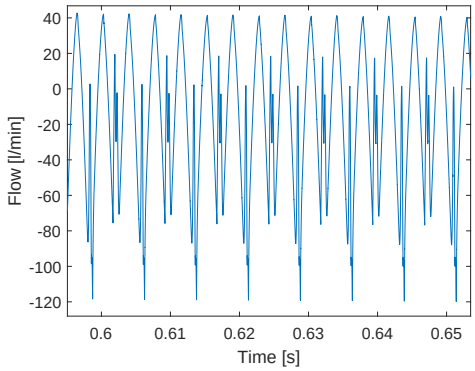

(a) Pump 1

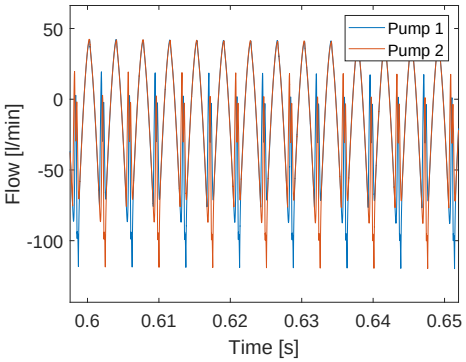

(b) Pump 1 and 2

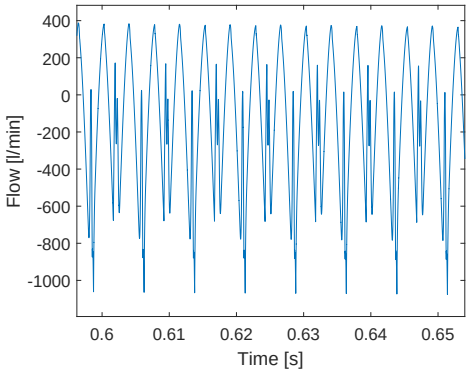

(c) Total flow in phase

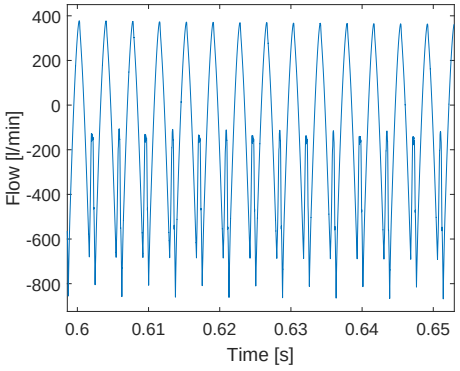

(d) Total flow 180° out of phase

Figure 12: Flows of a (a) single pump, (b) two out of phase pumps, (c) total flow of all pumps in phase and (d) out of phase

the extent to which these torque ripples are damped or resonated in the driven gearbox as a result of the interaction of the ripple frequencies with the drive-train's eigenmodes under typical operating conditions. For such an analysis, the gearbox component flexibilities would need to be modelled using a Multi-Body-Simulation (MBS) software. The end result of this analysis would be a derived load factor with which an ideal torque signal can be multiplied to produce the same effect on lifetime as the actual simulated drive torques without the need of time-intensive co-simulation of the drives and gearbox and which can aid in design.

Acknowledgments

The research presented in this paper has received funding from the Norwegian Research Council, SFI Offshore Mechatronics, project number 237896.

References

ABB. All-compatible ACS880 single drives. 2013. URL https://new.abb.com/drives/low-voltage-ac/industrial-drives/acs880-single-drives. Accessed: 2022-08-15.

Albers, P. *Motion Control in Offshore and Dredging*. Springer Netherlands, 2010. doi:10.1007/978-90-481-8803-1.

Aly, A. Model reference pid control of an electro- hydraulic drive. *International Journal of Intelligent Systems and Applications*, 2012. 4:24–32.

Begh, M. and Herzog, H.-G. Comparison of field oriented control and direct torque control. Technical report, 2018.

Bjonnes, T. and Moe, N. *Backslash in slew bearings: the advantages of an all-electric drive system*. Master's thesis, University of Agder, 2012. URL http://hdl.handle.net/11250/2446986.

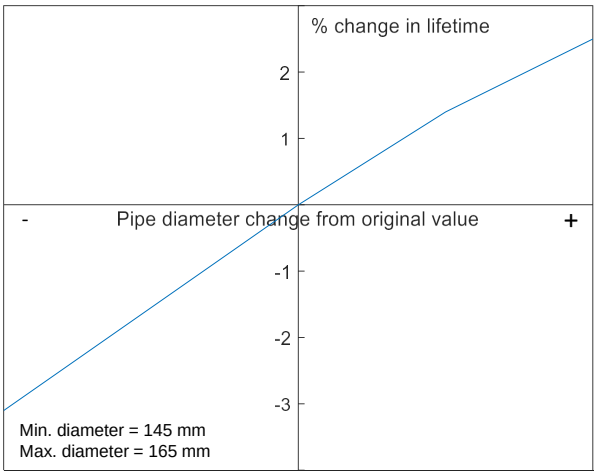

(a) Pipe diameter

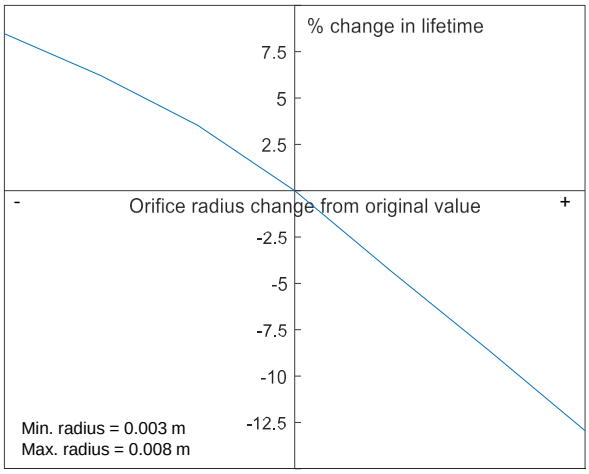

(b) Orifice radius

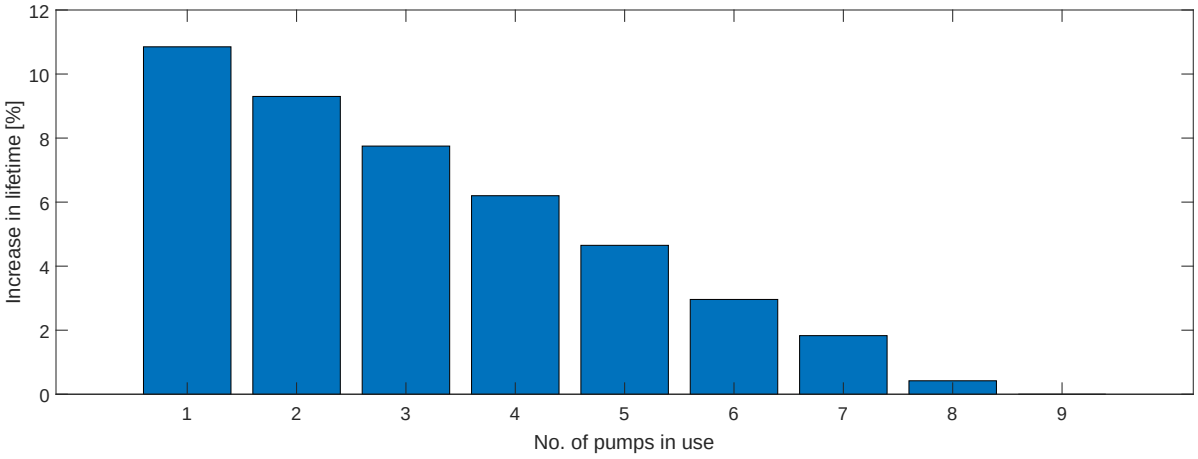

(c) Number of pumps

Figure 13: Effect diagrams for pipe diameter, orifice radius and number of pumps in use

Busca, C. *Open loop low speed control for PMSM in High Dynamic Applications*. Master's thesis, Aalborg University, 2010. URL https://projekter.aau.dk/projekter/files/32306486/Report_final.pdf.

Danfoss. Drives for marine winches and cranes. 2010. URL https://www.danfoss.com/en/markets/marine-and-offshore/dds/drives-for-marine-winches-and-cranes/#tab-overview. Accessed: 2022-08-15.

De Klerk, M. L. and Saha, A. K. Performance analysis of DTC-SVM in a complete traction motor control mechanism for a battery electric vehicle. *Heliyon*, 2022. 8(4). doi:10.1016/j.heliyon.2022.e09265.

Depenbrock, M. Direct self-control (DSC) of inverter-fed induction machine. *IEEE Trans. Power Electron.*, 1988. 3(4):420–429. doi:10.1109/63.17963.

Deppen, T. O., Alleyne, A. G., Stelson, K. A., and Meyer, J. J. Model predictive control of an electro-hydraulic powertrain with energy storage. In *ASME 2011 Dynamic Systems and Control Conference and Bath/ASME Symposium on Fluid Power and Motion Control, Volume 2*. ASMEDC, 2011.

DIN 3390. Calculation of load capacity of cylindrical gears; introduction and general influence factors. Standard, Beuth, 1987.

DIN ISO 281. Rolling bearings - dynamic load ratings and rating life. Standard, Beuth, 2010.

El Ouanjli, N., Derouich, A., El Ghzizal, A., Motahhir, S., Chebabhi, A., El Mourabit, Y., and Taoussi, M. Modern improvement techniques of direct torque control for induction motor drives - a review. *Prot. control mod. power syst.*, 2019a. 4(1). doi:10.1186/s41601-019-0125-5.

El Ouanjli, N., Motahhir, S., Derouich, A., El Ghzizal, A., Chebabhi, A., and Taoussi, M. Improved DTC strategy of doubly fed induction motor using fuzzy logic controller. *Energy rep.*, 2019b. 5:271–279. doi:10.1016j.egyr.2019.02.001.

Entao, Z., Wenlin, Y., and Junzhe, L. Predictive control of hydraulic winch motion control. In *2009 2nd IEEE International Conference on Computer Science and Information Technology*. IEEE, 2009.

Farsakoglu, T., Pedersen, H. C., and Andersen, T. O. Review of offshore winch drive topologies and control methods. 2022.

Gu, P., Walid, A. A., Iskandarani, Y., and Karimi, H. R. Modeling, simulation and design optimization of a hoisting rig active heave compensation system. *International Journal of Machine Learning and Cybernetics*, 2012. 4(2):85–98. doi:10.1007/s13042-012-0076-x.

Guan, C., Jiao, Z., and He, S. Theoretical study of flow ripple for an aviation axial-piston pump with damping holes in the valve plate. *Chinese Journal of Aeronautics*, 2014. 27(1):169–181. doi:10.1016/j.cja.2013.07.044.

Hiba, H., Ali, H., and Othmen, H. DTC-SVM control for three phase induction motors. In *2013 International Conference on Electrical Engineering and Software Applications*. IEEE, 2013. doi:10.1109/ICEESA.2013.6578421.

Ivantysyn, J. and Ivantysynova, M. *Hydrostatic pumps and motors: principles, design and performance, modeling, analysis, control and testing*. Tech Books International, 2003.

Kennel, R., El-refaei, A., Elkady, F., Mahmoud, S., and Elkholy, E. Torque ripple minimization for induction motor drives with direct torque control (DTC). In *The Fifth International Conference on Power Electronics and Drive Systems, 2003. PEDS 2003.* IEEE, 2004. doi:10.1109/PEDS.2003.1282756.

MacGregor. Offshore cranes. 2019. URL https://www.macgregor.com/Products/products/offshore-and-subsea-load-handling/offshore-cranes/. Accessed: 2022-08-08.

Mandal, N. P., Saha, R., and Sanyal, D. Theoretical simulation of ripples for different leading-side groove volumes on manifolds in fixed-displacement axial-piston pump. *Proc Inst Mech Eng Part I J Syst Control Eng*, 2008. 222(6):557–570. doi:10.1243/09596518JSCE580.

Mao, Y., Zuo, S., Wu, X., and Duan, X. High frequency vibration characteristics of electric wheel system under in-wheel motor torque ripple. *J. Sound Vib.*, 2017. 400:442–456. doi:10.1016/j.jsv.2017.04.011.

Mathworks. Simulate an AC motor drive. 2012. URL https://de.mathworks.com/help/physmod/sps/powersys/ug/simulating-an-ac-motor-drive.html. Accessed: 2022-08-07.

Neumann, S., Woell, L., Feldermann, A., Strassburger, F., and Jacobs, G. Modular system modeling for quantitative reliability evaluation of technical systems. *Modeling, Identification and Control: A Norwegian Research Bulletin*, 2016. 37(1):19–29. doi:10.4173/mic.2016.1.2.

Pasch, G., Jacobs, G., and Berroth, J. Nvh-systemsimulation eines traktors mit hydrostatisch-mechanischem leistungsverzweigungsgetriebe. 2020. doi:10.15150/lt.2020.3254.

Paul Forrer AG. Korrekte berechnung fr hydraulikleitungen. 2011. URL https://www.deutzforum.de/index.php?attachment/97119-berechnung-hydraulikleitung-d-pdf/. Accessed: 2022-09-09.

Slemon, G. R. Modelling of induction machines for electric drives. *IEEE Trans. Ind. Appl.*, 1989. 25(6):1126–1131. doi:10.1109/28.44251.

Sullivan, R. A., Davenport, M. R., and Clements, R. E. Multipurpose active/passive motion compensation system. In *Offshore Technology Conference*. Offshore Technology Conference, 1984. doi:10.4043/4737-MS.

Takahashi, I. and Noguchi, T. A new quick-response and high-efficiency control strategy of an induction motor. *IEEE Transactions on Industry Applications*, 1986. IA-22(5):820–827. doi:10.1109/TIA.1986.4504799.

del Toro, X., Jayne, M. G., Witting, P. A., Pou, J., Arias, A., and Romeral, J. L. New direct torque control scheme for induction motors. In *2005 European Conference on Power Electronics and Applications*. IEEE, 2005. doi:10.1109/EPE.2005.219544.

Uddin, M. N. and Hafeez, M. FLC based DTC scheme to improve the dynamic performance of an IM drive. In *2010 IEEE Industry Applications Society Annual Meeting*. IEEE, 2010. doi:10.1109/IAS.2010.5614089.

Woell, L., Feldermann, A., and Jacobs, G. Sensitivity analysis on the reliability of an offshore winch regarding selected gearbox parameters. *Modeling, Identification and Control: A*

Norwegian Research Bulletin, 2017. 38(2):51–58. doi:10.4173/mic.2017.2.1.

Woell, L., Jacobs, G., and Kramer, A. Lifetime calculation of irregularly oscillating bearings in offshore winches. *Modeling, Identification and Control: A Norwegian Research Bulletin*, 2018. 39(2):61–72. doi:10.4173/mic.2018.2.2.

Woodacre, J., Bauer, R., and Irani, R. A review of vertical motion heave compensation systems. *Ocean Engineering*, 2015. 104:140–154. doi:10.1016/j.oceaneng.2015.05.004.

Xia, Y. Y., Fletcher, J. E., Finney, S. J., Ahmed, K. H., and Williams, B. W. Torque ripple analysis and reduction for wind energy conversion systems using uncontrolled rectifier and boost converter. *IET Renew. Power Gener.*, 2011. 5(5):377. doi:10.1049/iet-rpg.2010.0108.

Yousri, M., Jacobs, G., and Neumann, S. Impact of fiber versus steel ropes on the lifetime of crane winches. *Modeling, Identification and Control: A Norwegian Research Bulletin*, 2020. 41(3):129–139. doi:10.4173/mic.2020.3.1.

Zhang, B., Ma, J., Hong, H., Yang, H., and Fang, Y. Analysis of the flow dynamics characteristics of an axial piston pump based on the computational fluid dynamics method. *Eng. Appl. Comput. Fluid Mech.*, 2017. 11(1):86–95. doi:10.1080/19942060.2015.1091686.